

**EVOLUTION OF SURFACE FAILURE  
MECHANISMS IN Zr-ALLOYS UNDER  
CONTROLLED CONDITIONS**

**BHARAT KUMAR**



**CENTRE FOR AUTOMOTIVE RESEARCH AND  
TRIBOLOGY (FORMERLY ITMMEC)**

**INDIAN INSTITUTE OF TECHNOLOGY DELHI**

**June 2024**

© Indian Institute of Technology Delhi (IITD), New Delhi, 2024

# Evolution of surface failure mechanisms in Zr-alloys under controlled conditions

by

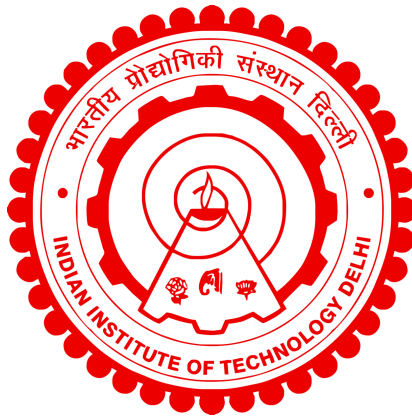
**BHARAT KUMAR**

Centre for Automotive Research and Tribology (Formerly ITMMEC)

submitted

in partial fulfillment of the requirements of the degree of Doctor of Philosophy

to the



**INDIAN INSTITUTE OF TECHNOLOGY  
DELHI**

**June 2024**


*Dedicated to my parents,  
Mr. Bhikam Singh and Mrs. Rakesh Devi*

# Certificate

This is to certify that the thesis entitled “**Evolution of surface failure mechanisms in Zr-alloys under controlled conditions**”, submitted by **Mr. Bharat Kumar** to the Indian Institute of Technology Delhi, for the award of the degree of **Doctor of Philosophy**, is a record of the original, bonafide research work carried out by him under our supervision and guidance. The thesis has reached the standards fulfilling the requirements of the regulations related to the award of the degree.

The results contained in this thesis have not been submitted in part or in full to any other University or Institute for the award of any degree or diploma to the best of our knowledge.

**Dr. Deepak Kumar**  
Professor and Head  
Centre for Automotive Research and  
Tribology,  
Indian Institute of Technology Delhi.

  
20/06/2024  
**Dr. Vijay Chaudhry**  
Scientific officer-H  
Department of Atomic Energy,  
Nuclear Power Corporation of India  
Limited, Mumbai.

# *Acknowledgements*

First, I would like to thank God for helping me believe in myself. I am very thankful and lucky to have such supportive parents; completing this journey wouldn't have been possible without their blessings and support. I am very grateful to my Mama Ji for their guidance and support at every step of my academic journey. I want to thank and express my appreciation to my supervisors (Prof. Deepak Kumar and Dr. Vijay Chaudhry) for their guidance and support at every step of this journey. Their motivation and unique perspectives towards the research built the research person in me. With the ocean of knowledge, they guided me to solve various hurdles during this journey. I am also very thankful to my family and relatives for supporting me to make it possible.

I want to thank my SRC members (Prof. S. Fatima, Prof. H. Kanchwala and Prof. R. K. Pandey) for their helpful suggestions during the semester progress presentations.

I am very thankful to Prof. Nitya Nand Gosvami, Prof. Suresh Neelakantan, Prof. Jayant Jain, Prof. Lakshmi Narayan Ramasubramanian and Prof. Dinesh Kalyanasundaram for providing me with various facilities to perform various analyses and experiments. I am also thankful to Prof. M. F. Wani and Prof. Kamlesh Kumari for helping me understand various fundamentals.

I am grateful to the Nano Research Facility (NRF) and Central Research Facility (CRF), Indian Institute of Technology Delhi, for providing me with various facilities to perform various analyses and experiments.

I am very thankful to Dr. Harprabhjot Singh, Dr. A.P.S. Lodhi, Dr. Ankit Saxena, Dr. Meghashree Padhan and Dr. Avi Gupta for guiding various analyses used in this research study. I want to thank my lab mates, Abhijit Pattnayak, Abhijith N.V., Gazal Gupta and Arun G., for supporting me in performing various lab experiments. I am thankful to the staff of the center, Mr. Ved Singh, Mr. Shripal Singh, and Mr. Hitesh and Mr. Lokesh, for helping in completing various official works. I am also thankful to my other colleagues, Abhishek, Astha, Himanshu, Subhakar, Rashmi and Priyanka, for helping me perform various experiments and analyses.

Having good friends is very important in everyone's life. I want to thank my friends Vijay, Neha, Govind, Sanjay, Siddhant, Varun, Sumit, Nishant, Sahil, Hitesh, Lakhan, Pallav, Paras, Monu, Shitanshu, Makhan, Kamal Deep, Shikha, Raj, Avneesh, Arjun, Jobin, Shakti, Mridul, Veg, Viney, Gaurav, Arun and Abhishek for supporting me mentally in my hard times and celebrating my good times.

# *Abstract*

Zirconium alloys (Zr-alloys) are used in many engineering applications (such as nuclear reactors, bioimplants, chemical processing industries, etc.) due to their low absorption cross-section to thermal neutrons, good mechanical properties and good corrosion resistance. Based on these qualities, zirconium alloys are widely used as nuclear core structural material. During the operation of the nuclear reactor, some of the core components are subjected to fluid flow-induced vibrations, which may result in surface degradation, viz., material wear, delamination, spalling etc., depending on the contact conditions prevailing at the contact interface. Mechanical loading parameters such as frequency, normal load, displacement amplitude and number of cycles/test durations control the degradation mechanism under a given set of environmental conditions. The prevailing environment at the contact interface, temperature, water chemistry, etc., significantly contributes to the degradation process. Some components are exposed to the coolant water having LiOH, resulting in the corrosion and fretting corrosion of the components. The work presented in the thesis quantifies the effect of mechanical loadings and the environment on the degradation mechanisms prevailing at the contact interface. The study also determines the effect of the alkalinity of water and exposure duration on the corrosion behavior of Zr-alloys. Materials considered in the study are Zr alloys (Zr-4, Zr-2.5 Nb) and Stainless Steel (SS-410). Comprehensive investigations have been carried out to identify the wear mechanisms involved in the degradation process.

Reciprocating wear experiments were performed by varying the reciprocating test duration/number of cycles, frequency, and displacement amplitude. Experiments were performed using a cross-cylinder configuration under dry and water-submerged conditions. Friction and wear response were recorded in terms of coefficient of friction (COF) and normalized wear depth, respectively. Worn surfaces were analyzed using Field Emission Scanning Electron Microscopy (FESEM), Energy Dispersive Spectroscopy (EDS), Raman Spectroscopy and X-ray Photoelectron Spectroscopy (XPS) to quantify the prevailing wear mechanisms and the associated phenomenon.

In the case of self-mated zircaloy-4 (Zr-4 alloy) fretting wear, COF increases with increasing fretting duration but decreases with increasing frequency and amplitude under dry conditions. COF remains nearly constant w.r.t. the fretting duration,

frequency and amplitude under submerged condition. COF and normalized wear depth are lower under water-submerged conditions than that under dry conditions. Normalized wear increases significantly with increasing amplitude under both submerged and non-submerged conditions. With increasing amplitude, the wear mechanism changes from adhesion (under fretting) to mixed adhesion-abrasion. The studies show that the tribo-oxide layer formed on the wear surface controls the wear mechanism prevailing at the contact interface.

Reciprocating wear tests at low displacement amplitudes were conducted between Zr-2.5Nb alloy and SS-410 at Room Temperature (RT) and High Temperature (HT). COF is higher at HT (260 °C) than at RT. COF decreases with increasing reciprocating frequency and displacement amplitude but remains nearly constant with increasing duration. The sp. wear rate is higher at RT than that at HT. Sp. wear rate decreases with increasing the reciprocating duration and frequency but increases with increasing the displacement amplitude. The wear mechanism changes from adhesion to mixed adhesion-abrasion with increasing amplitude. Here, also tribo-oxide layer (mechanically mixed layer) is also formed at the worn surfaces.

To observe the effect of hydride formation on the tribological response of Zr-2.5Nb alloy, fretting wear experiments were conducted between hydrogen-charged Zr-2.5Nb (Hydrided Zr-2.5Nb) and SS-410 and compared the friction and wear response with that of uncharged Zr-2.5Nb (Unhydrided Zr-2.5Nb) alloy. The COF is observed lower for hydrided Zr-2.5Nb (Zr-2.5Nb-H) alloy than that for unhydrided (as-received) Zr-2.5Nb (Zr-2.5Nb) alloy. To observe the tribological response of the hydride (Zr-H) phase, tribo-experiments were also conducted using Atomic Force Microscopy (AFM) with Diamond-Like Carbon (DLC) tip. The friction force during AFM tribology is higher on the Zr-H phase than on the Zr-matrix and Zr-2.5Nb alloy.

To study the corrosion response of Zr-alloys, electrochemical corrosion experiments were conducted on Zr-4, Zr-2.5Nb and Zr-2.5Nb-H alloy in the aqueous solution of LiOH. Electrochemical Impedance Spectroscopy (EIS) and potentiodynamic polarization studies were performed for varied concentrations (conc.) of LiOH and exposure durations. Measurements were recorded in terms of impedance, corrosion potential, and corrosion current. The studies showed that the corrosion resistance increases with the increasing exposure duration and decreases with the increasing concentration of LiOH in the water. An oxide layer is observed to form on the

surface of the Zr-alloys during the corrosion process, which protects the substrate from further corrosion. The corrosion resistance of Zr-2.5Nb-H alloy is observed to be lower than that of Zr-2.5Nb alloy. Zr-4 alloy shows slightly more corrosion resistance than Zr-2.5Nb alloy for the same environment.

## सारांश

ज़िर्कोनियम मिश्रधातुओं (Zr-alloys) का उपयोग कई अभियांत्रिकी क्षेत्रों में जाता है (जैसे परमाणु भट्टी, जैव-प्रत्यारोपण, रासायनिक प्रसंस्करण उद्योग आदि), इनकी थर्मल न्यूट्रॉन्स का कम अवशोषण क्रॉस-सेक्शन, अच्छे यांत्रिकी गुणधर्म और अच्छी जंग सहिष्णुता के कारण। इन गुणधर्मों के आधार पर, ज़िर्कोनियम मिश्रधातु न्यू-क्लियर कोर संरचनात्मक सामग्री के रूप में व्यापक रूप से प्रयोग की जाती हैं। परमाणु भट्टी के परिचालन के दौरान, संपर्क स्थिति में कुछ मुख्य अंगों को तरल प्रवाह इंदुकित कंपन का सामना करना पड़ता है, जो सतह के विघटन, जैसे सामग्री घिसाव, अलगाव, टूटना आदि, पर निर्भर करता है। यांत्रिकी भार और पर्यावरण घातक प्रक्रियाओं में महत्वपूर्ण भूमिका निभाते हैं। यांत्रिकी भार जैसे आवृत्ति, भार, स्थानांतरण आयाम और चक्रों की संख्या/परीक्षण अवधि दिए गए पर्यावरणीय ढंगों के अधीन विघटन प्रक्रिया को नियंत्रित करते हैं। संपर्क स्थिति पर वर्तमान पर्यावरण, तापमान, जल रसायन, आदि, विघटन प्रक्रिया में महत्वपूर्ण योगदान करते हैं। कुछ अंग लिथियम हाइड्रॉक्साइड युक्त शीतलक पानी के संपर्क में रहते हैं, जिससे घटकों में जंग और फ्रेटिंग जंग होता है। थ्रीसिस में प्रस्तुत काम विघटन प्रक्रिया पर यांत्रिकी भार और पर्यावरण के प्रभाव को मापता है, जो संपर्क स्थिति पर प्राथिक रूप से प्राधान्य रखता है। अध्ययन यह भी निर्धारित करता है कि पानी की क्षारीयता और संपर्क अवधि का ज़िर्कोनियम मिश्रधातुओं के जंग व्यवहार पर क्या प्रभाव पड़ता है। अध्ययन में ध्यान दिए जाने वाले पदार्थ ज़िर्कोनियम मिश्रधातु (Zr-4, Zr-2.5Nb) और स्टेनलेस स्टील (एसएस-410) हैं। विघटन क्रिया में शामिल घिसाव प्रक्रियाओं की पहचान के लिए व्यापक अन्वेषण किए गए हैं।

प्रत्यागामी घिसाव परिक्षणों को परीक्षण अवधि / चक्रों की संख्या, आवृत्ति और स्थानांतरण आयाम को बदलकर किया गया। परिक्षण सूखी और जल-तटस्थ स्थिति के तहत लंबवत्-बेलन विन्यास का उपयोग करके किया गया। घर्षण और घिसाई प्रतिक्रिया को घर्षण संख्यावाची और मानकीकृत घिसाई गहराई के रूप में दर्ज किया गया। घिसाई हुई सतहें क्षेत्रीय-उत्सर्जन क्रमवीक्षण इलेक्ट्रॉन माइक्रोस्कोपी (एफइएसइएम), ऊर्जा प्रसार स्पेक्ट्रोस्कोपी (इडीएस), रमन स्पेक्ट्रोस्कोपी और एक्स-रे फोटोइलेक्ट्रॉन स्पेक्ट्रोस्कोपी (एक्सपीएस) का उपयोग करके वर्तमान घिसाई अधीन विघटन प्रक्रियाओं और संबंधित घटना को मापने के लिए विश्लेषित किया गया।

आत्म संगमित ज़िरकॉनियम-4 (Zr-4 मिश्रधातु) फ्रेटिंग घिसाई (सूखी स्थिति) में, घर्षण संख्यावाची बढ़ती फ्रेटिंग अवधि के साथ बढ़ता है, लेकिन फ्रेटिंग आवृत्ति और आयाम के साथ घटता है। जल-तटस्थ स्थिति के तहत फ्रेटिंग अवधि, आवृत्ति और आयाम के साथ घर्षण संख्यावाची लगभग स्थिर रहता है। जल-तटस्थ स्थिति में घर्षण संख्यावाची और प्रतिकृत घिसाई गहराई सूखी स्थिति की तुलना में कम है। जलतटस्थ और सूखी दोनों स्थितियों में आयाम बढ़ाने के साथ प्रतिकृत घिसाई बढ़ती है। आयाम बढ़ने के साथ, घिसाई प्रक्रिया आग्रहण (फ्रेटिंग के अन्तर्गत) से मिश्रित आग्रहण-खरोच में परिवर्तित होती है। अध्ययन दिखाते हैं कि घिसाई सतह पर ट्राइबो-ऑक्साइड परत संपर्क स्थिति पर वर्तमान घिसाई प्रक्रिया को नियंत्रित करता है।

Zr-2.5Nb मिश्रधातु और एसएस-410 के बीच कमरे के तापमान (आरटी) और उच्च तापमान (एचटी) पर न्यून आयाम के प्रत्यागामी घिसाई परीक्षण किए गए। उच्च तापमान (260 °C) पर घर्षण संख्यावाची अधिक है कमरे के तापमान की तुलना में। घर्षण संख्यावाची बढ़ते हुए प्रत्यागामी आवृत्ति और स्थानांतरण आयाम के साथ कम होता है, लेकिन बढ़ती हुई अवधि के साथ लगभग स्थिर रहता है। अंतर्निहित घिसाई दर प्रत्यागामी अवधि और आवृत्ति के साथ घटती है, लेकिन स्थानांतरण आयाम के साथ बढ़ती है। घिसाई प्रक्रिया आयाम बढ़ने के साथ आग्रहण से मिश्रित आग्रहण-खरोंच में परिवर्तित होती है। यहाँ, घिसाई दर पर ट्राइबो-ऑक्साइड परत (यंत्रवत् मिश्रित परत) बन जाती है।

Zr-2.5Nb मिश्रधातु की ट्राइबोलॉजिकल प्रतिक्रिया पर हाइड्राइड बनने के प्रभाव को देखने के लिए, हाइड्रोजन आवेशित (हाइड्राइडेड) Zr-2.5Nb और एसएस-410 के बीच फ्रेटिंग परीक्षण किए गए और अनावेशित (अनहाइड्राइडेड) Zr-2.5Nb मिश्रधातु के साथ तुलना की गई। अनहाइड्राइडेड Zr-2.5Nb मिश्रधातु की तुलना में हाइड्राइडेड Zr-2.5Nb मिश्रधातु पर घर्षण संख्यावाची कम पाया जाता है। हाइड्राइड (Zr-H) अवस्था की ट्राइबोलॉजिकल प्रतिक्रिया को देखने के लिए, एटॉमिक फोर्स माइक्रोस्कोपी (एएफएम) का उपयोग करके ट्रायबो-परिक्षण भी किए गए, जिसमें डायमंड-लाइक कार्बन (डीएलसी) टिप का उपयोग किया गया। एएफएम ट्राइबोलॉजी के दौरान घर्षण बल Zr-H अवस्था पर Zr-आव्यूह और Zr-2.5Nb मिश्रधातु की तुलना में अधिक है।

ज़िकॉनियम मिश्रधातुओं की जंग प्रतिक्रिया का अध्ययन करने के लिए, लिथियम हाइड्रॉक्साइड के जलीय घोल में Zr-4, Zr-2.5Nb और Zr-2.5Nb-H मिश्रधातु पर विद्युतरसायनिक जंग परीक्षण किए गए। विभिन्न सान्द्रता और संपर्क अवधि के लिए इलेक्ट्रोकेमिकल इम्पेडेंस स्पेक्ट्रोस्कोपी (ईआईएस) और पोटेंशिओडायनामिक पोलराइज़ेशन अध्ययन किए गए। मापन विधियों को प्रतिरोध, जंग क्षमता, और जंग प्रवाह के रूप में नोट किया गया। अध्ययन दिखाते हैं कि जंग प्रतिरोध विकास बढ़ती संपर्क अवधि के साथ बढ़ता है और पानी में लिथियम हाइड्रॉक्साइड की बढ़ती सान्द्रता के साथ घटता है। जंग प्रक्रिया के दौरान ज़िकॉनियम मिश्रधातुओं की सतह पर एक ऑक्साइड परत देखी जाती है, जो उपभूमि को आगे के जंग से बचाता है। Zr-2.5Nb-H मिश्रधातु का जंग प्रतिरोध Zr-2.5Nb मिश्रधातु से कम पाया जाता है। Zr-4 मिश्रधातु उसी वातावरण के लिए Zr-2.5Nb मिश्रधातु से थोड़ा अधिक जंग प्रतिरोध दिखाता है।

# Contents

Certificate	i
Acknowledgements	ii
Abstract	iv
सारांश	vii
Contents	ix
List of Figures	xiii
List of Tables	xviii
Abbreviations	xix
Symbols	xxi
<b>1 Introduction</b>	<b>1</b>
1.1 Zirconium alloys: Development and applications . . . . .	1
1.2 Zirconium alloys: Key materials for nuclear reactor's core . . . . .	3
1.3 Wear damage . . . . .	5
1.4 Corrosion damage . . . . .	7
1.5 Hydride formation (hydriding) . . . . .	8
1.6 Motivation . . . . .	9
<b>2 Literature review</b>	<b>11</b>
2.1 Tribological behavior of zirconium alloys . . . . .	11
2.2 Corrosion behavior of zirconium alloys . . . . .	14
2.3 Effect of hydride formation on the properties of zirconium alloys . . . . .	17

2.4	Summary of literature review . . . . .	19
2.5	Problem formulation . . . . .	20
2.6	Research objectives . . . . .	21
<b>3</b>	<b>Experimental Methods</b>	<b>23</b>
3.1	Material and specimen preparation . . . . .	23
3.2	Autoclaving . . . . .	25
3.3	Hydrogen charging . . . . .	25
3.4	Microstructure analyses . . . . .	25
3.5	Physical and chemical characterizations . . . . .	26
3.5.1	Density and weight loss measurement . . . . .	26
3.5.2	Wettability analysis . . . . .	26
3.5.3	The pH measurement . . . . .	27
3.6	Mechanical characterizations . . . . .	27
3.6.1	Micro-indentation . . . . .	27
3.6.2	Nano-indentation . . . . .	27
3.7	Tribological Characterizations . . . . .	28
3.7.1	Self-mated Zr-4 . . . . .	28
3.7.2	Zr-2.5Nb/SS-410 . . . . .	29
3.7.3	Micro-tribology . . . . .	30
3.7.4	Nano-tribology . . . . .	30
3.7.5	Wear measurement . . . . .	30
3.8	Electrochemical corrosion analysis . . . . .	31
3.9	Morphological analyses . . . . .	34
3.10	Elemental analysis . . . . .	35
3.11	Phase analyses . . . . .	35
3.11.1	Raman spectroscopy . . . . .	35
3.11.2	X-ray Photon Spectroscopy (XPS) . . . . .	35
3.11.3	X-ray Diffraction (XRD) analysis . . . . .	36
<b>4</b>	<b>Tribological study on self-mated Zr-4 alloy under dry and water-submerged conditions</b>	<b>37</b>
4.1	Results . . . . .	38
4.1.1	Microstructure analysis . . . . .	38
4.1.2	Phase analysis . . . . .	38
4.1.3	Mechanical characterization . . . . .	39
4.1.4	Friction response . . . . .	40
4.1.5	Wear response . . . . .	40
4.1.6	Worn surface characterization . . . . .	41
4.2	Discussion . . . . .	47
4.3	Conclusions . . . . .	56

<b>5</b>	<b>Tribological study on Zr-2.5Nb alloy slid against SS-410 steel at RT and HT (260 °C)</b>	<b>59</b>
5.1	Results . . . . .	60
5.1.1	Microstructure analysis . . . . .	60
5.1.2	Characterizations of autoclave layer . . . . .	60
5.1.3	Hardness and density . . . . .	61
5.1.4	Friction response . . . . .	62
5.1.5	Wear response . . . . .	62
5.1.6	Worn surface characterization . . . . .	63
5.2	Discussion . . . . .	71
5.3	Conclusions . . . . .	77
<b>6</b>	<b>Effect of hydrogen charging on the tribological response of Zr-2.5Nb alloy slid against SS-410 steel</b>	<b>79</b>
6.1	Results . . . . .	80
6.1.1	Phase analysis . . . . .	80
6.1.2	Mechanical characterizations . . . . .	80
6.1.3	Physical characterization . . . . .	83
6.1.4	Tribological response . . . . .	83
6.2	Discussion . . . . .	86
6.3	Conclusions . . . . .	88
<b>7</b>	<b>Corrosive degradation of different Zr-alloys in aqueous LiOH solution</b>	<b>91</b>
7.1	Corrosion response of Zr-4 alloy . . . . .	92
7.1.1	Electrochemical Impedance Spectroscopy (EIS) . . . . .	92
7.1.2	Potentiodynamic polarization study . . . . .	95
7.1.3	Morphological and elemental analysis of corroded surfaces . . . . .	97
7.2	Corrosion response of Zr-2.5Nb alloy . . . . .	97
7.2.1	Electrochemical Impedance Spectroscopy (EIS) . . . . .	97
7.2.2	Potentiodynamic polarization study . . . . .	100
7.2.3	Phase analysis of corroded surface . . . . .	102
7.2.4	Morphological and elemental analysis of corroded surfaces . . . . .	102
7.3	Corrosion response of Zr-2.5Nb-H alloy . . . . .	104
7.3.1	Microstructural analysis . . . . .	104
7.3.2	Electrochemical Impedance Spectroscopy (EIS) . . . . .	106
7.3.3	Potentiodynamic polarization study . . . . .	107
7.3.4	Morphological and elemental analysis of corroded surfaces . . . . .	108
7.4	Discussion . . . . .	109
7.5	Conclusions . . . . .	113
<b>8</b>	<b>Conclusions and future scope</b>	<b>115</b>

*Contents*

---

8.1	Conclusions . . . . .	115
8.2	Future scope . . . . .	116

# List of Figures

1.1	CANDU reactor’s core (a schematic representation). . . . .	5
2.1	Schematic representation of the contact between tube and spring [1].	12
2.2	Transition of wear regime with increasing displacement amplitude [2].	13
2.3	Increasing oxide layer thickness with exposure duration: (a) 504 h; and (b) 3024 h. [3] . . . . .	16
3.1	Schematic illustration of tribo-pair (self-mated Zr-4 alloy, cross-cylinder configuration). . . . .	24
3.2	Images of specimens and tribo-pair configuration (Zr-2.5Nb/SS-410).	24
3.3	Schematic illustration of Universal Tribo-meter. . . . .	29
3.4	Schematic illustration of wear depth evaluation. . . . .	31
3.5	General representation of the relation between the Nyquist plot and electrical equivalent circuit. . . . .	32
3.6	General representation of a Tafel plot. . . . .	34
4.1	Optical microscopic image of as received Zr-4 alloy revealing its microstructure. . . . .	38
4.2	XRD spectrum of as received Zr-4 alloy. . . . .	39
4.3	load/displacement curve obtained during nanoindentation for: (a) Zr-4 alloy and (b) SS-410. . . . .	40
4.4	Avg. COF w.r.t.: (a) Fretting duration; (b) Fretting frequency; and (c) Displacement amplitude. . . . .	41
4.5	Normalized wear depth w.r.t.: (a) Fretting duration; (b) Fretting frequency; and (c) Displacement amplitude. . . . .	41
4.6	SEM micrographs and EDS maps of worn surfaces: (a) After a fretting duration of 1 hour under dry condition; (b) After a fretting duration of 4 hours under dry condition; (c) After a fretting duration of 1 hour under submerged condition; and (d) After a fretting duration of 4 hours under submerged condition. . . . .	43

4.7	3D profile micrographs of the worn surfaces: (a) After a fretting duration of 1 hour under dry condition; (b) After a fretting duration of 4 hours under dry condition; (c) After a fretting duration of 1 hour under submerged condition; and (d) After a fretting duration of 4 hours under submerged condition. . . . .	44
4.8	SEM micrographs and EDS maps of worn surfaces at a frequency of 6.5 Hz: (a) Under dry condition; and (b) Under submerged condition. . . . .	44
4.9	3D profile micrographs of the worn surfaces at a frequency of 6.5 Hz: (a) Under dry condition; and (b) Under submerged condition. . . . .	45
4.10	SEM micrographs and EDS maps of worn surfaces at a displacement amplitude of 400 $\mu\text{m}$ : (a) Under dry condition; and (b) Under submerged condition. . . . .	46
4.11	3D profile micrographs of the worn surfaces at a displacement amplitude of 400 $\mu\text{m}$ : (a) Under dry condition; and (b) Under submerged condition. . . . .	46
4.12	Schematic diagram showing the effect of displacement amplitude on wear mechanism. . . . .	49
4.13	Raman spectrum of worn surfaces of Zr-4 alloy at a displacement amplitude: (a) 100 $\mu\text{m}$ ; (b) 400 $\mu\text{m}$ . . . . .	50
4.14	XPS spectrum of worn surface: (a) Zr 3d spectrum; and (b) O 1s spectrum. . . . .	51
4.15	Schematic illustration of the mechanism of tribo-oxide formation. . . . .	52
4.16	Schematic representation of increasing COF with fretting duration: (a) smaller real contact area, $a_1$ ; and (b) larger real contact area . . . . .	53
4.17	FESEM micrographs of wear debris generated at displacement amplitude of: (a) 100 $\mu\text{m}$ ; and (b) 400 $\mu\text{m}$ . . . . .	54
4.18	FESEM micrographs and corresponding EDS maps of wear debris generated at displacement amplitude of 400 $\mu\text{m}$ . . . . .	54
4.19	FESEM micrographs and EDS maps of worn surfaces of Zr-4 and SS-410 in dry condition. . . . .	55
4.20	Wettability analysis of Zr-4 surface: (a) Contact angle analysis of as received Zr-4 sample; (b) Schematic illustration of an adsorbed layer of water on the hydrophilic surface of Zr-4 sample. . . . .	56
5.1	FESEM micrograph of the microstructure of Zr-2.5Nb alloy. . . . .	60
5.2	XRD spectrum of Zr-2.5Nb alloy (autoclaved). . . . .	61
5.3	Sectional view of Zr-2.5Nb alloy (autoclaved): (a) FESEM micrograph; and (b) & (c) corresponding EDS maps. . . . .	61
5.4	Variation of COF w.r.t.: (a) Sliding duration (frequency= 5 Hz & amplitude= 200 $\mu\text{m}$ ); (b) Reciprocating frequency (amplitude= 200 $\mu\text{m}$ ); and (c) Displacement amplitude (frequency= 5 Hz). . . . .	62
5.5	Specific wear rate w.r.t.: (a) Sliding duration, (b) Reciprocating frequency, and (c) Displacement amplitude. . . . .	63

5.6	FESEM micrographs and corresponding EDS maps of the worn surfaces after 1 hour of sliding duration at 200 $\mu\text{m}$ amplitude and 5 Hz frequency and; (a) Zr-2.5Nb at RT; (b) SS-410 at RT; (c) Zr-2.5Nb at 260 $^{\circ}\text{C}$ ; and (d) SS-410 at 260 $^{\circ}\text{C}$ . . . . .	65
5.7	FESEM micrographs and corresponding EDS maps of the worn surfaces after 3 hours of sliding duration at 200 $\mu\text{m}$ amplitude and 5 Hz frequency; (a) Zr-2.5Nb at RT and (b) SS-410 at RT; (c) Zr-2.5Nb at 260 $^{\circ}\text{C}$ and (d) SS-410 at 260 $^{\circ}\text{C}$ . . . . .	66
5.8	3D profile micrographs of the worn surfaces at 200 $\mu\text{m}$ amplitude and 5 Hz frequency; (a) After 1 hour of sliding duration at RT; (b) After 1 hour of sliding duration at 260 $^{\circ}\text{C}$ ; (c) After 3 hours of sliding duration at RT; and (d) After 3 hours of sliding duration at 260 $^{\circ}\text{C}$ . . . . .	67
5.9	FESEM micrographs and corresponding EDS maps of worn surfaces collected at 200 $\mu\text{m}$ amplitude and 25 Hz frequency after 1 hr of sliding; (a) Zr-2.5Nb at RT; (b) SS-410 at RT; (c) Zr-2.5Nb at 260 $^{\circ}\text{C}$ ; and (d) SS-410 at 260 $^{\circ}\text{C}$ . . . . .	68
5.10	3D profile micrographs of worn surfaces at 200 $\mu\text{m}$ amplitude and 25 Hz frequency after 1 hr of sliding; (a) At RT and (b) At 260 $^{\circ}\text{C}$ . . . . .	68
5.11	FESEM and EDS maps of worn surfaces at 600 $\mu\text{m}$ amplitude and 5 Hz frequency after 1 hr of sliding; (a) Zr-2.5Nb at RT and (b) SS-410 at RT; (c) Zr-2.5Nb at 260 $^{\circ}\text{C}$ and (d) SS-410 at 260 $^{\circ}\text{C}$ . . . . .	69
5.12	3D profile micrographs of worn surfaces at 600 $\mu\text{m}$ amplitude and 5 Hz frequency after 1 hr of sliding; (a) At RT and (b) At 260 $^{\circ}\text{C}$ . . . . .	70
5.13	Raman Spectrum of the Zr-2.5Nb alloy:(a) Unworn surface; (b) worn surface. . . . .	71
5.14	Schematic illustration of the possible adhesive wear mechanism involved during the tribological interaction of SS410 steel and Zr-2.5Nb alloy. . . . .	73
5.15	FESEM micrograph of the wear debris generated during the wear of Zr-2.5Nb at 200 $\mu\text{m}$ displacement amplitude. . . . .	73
5.16	FESEM micrograph of the worn surface of Zr-2.5Nb alloy showing the tribo-sintering of wear debris. . . . .	74
5.17	FESEM micrograph of the worn surface of Zr-2.5Nb alloy showing the layered material deposition. . . . .	75
5.18	Schematic diagram illustrating the layered material transfer and deposition during the tribological interaction of SS410 steel and Zr-2.5Nb alloy. . . . .	75
6.1	XRD spectrum of: (a) Zr-2.5Nb alloy; and (b) Zr-2.5Nb-H alloy. . . . .	81
6.2	Optical micrographs of micro-indent on Zr-2.5Nb alloy:(a) Zr-2.5Nb; and (b) Zr-2.5Nb-H. . . . .	82
6.3	Load-displacement curve for Zr-2.5Nb during nanoindentation before and after hydride formation. . . . .	82

6.4	(a) Friction response; and (b) Wear response. . . . .	83
6.5	FESEM micrographs and corresponding EDS maps of worn surfaces of Zr-2.5Nb alloy after (a) 1 hour; (b) 2 hours; and (c) 3 hours. . . . .	84
6.6	ESEM micrographs and corresponding EDS maps of worn surfaces of Zr-2.5Nb-H alloy after (a) 1 hour; (b) 2 hours; and (c) 3 hours. . . . .	85
6.7	(a) AFM microscopic image; (b) Friction map of Zr-2.5Nb-H; (c) Friction map of Zr-matrix in Zr-2.5Nb-H; (d) Friction map of Zr-2.5Nb; (e) Friction map of Zr-H phase in Zr-2.5Nb-H; and (f) variation of friction force w.r.t. sampling length. . . . .	86
6.8	FESEM micrographs of the worn surfaces of SS-410 showing the presence of Fe <sub>80</sub> Zr <sub>10</sub> Cr <sub>10</sub> alloy. . . . .	88
7.1	EIS plots: (a) Nyquist plots; and (b) Bode plots. . . . .	93
7.2	Electrical equivalent circuit for the EIS for the medium without LiOH (7 pH). . . . .	93
7.3	Electrical equivalent circuit for fitting the EIS data for the water with LiOH (10.4 pH) and LiOH (11.4 pH) concentration . . . . .	94
7.4	Potentiodynamic polarization plots: (a) Variation of OCP with time; and (b) Tafel plots. . . . .	96
7.5	FESEM micrographs and corresponding EDS maps of the corroded surfaces of Zr-4 alloy in the water having: (a) 0 M LiOH; (b) 0.2 M LiOH; and (c) 5 M LiOH. . . . .	98
7.6	EIS plots: (a) Nyquist plots for different concentrations of LiOH in the water and for different exposure durations; (b) Bode (magnitude and phase) plots for different concentrations of LiOH in the water. . . . .	99
7.7	(a) Variation of OCP with time; and (b) Tafel plots. . . . .	101
7.8	The XPS spectrum obtained for corroded surface of Zr-2.5Nb alloy in the water having 0.2 M LiOH. . . . .	103
7.9	FESEM micrographs and corresponding EDS maps of the corroded surfaces of Zr-2.5Nb alloy in the water having: (a) 0 M LiOH; (b) 0.2 M LiOH; and (c) 5 M LiOH. . . . .	104
7.10	FESEM micrographs of corroded surface of Zr-2.5Nb showing the morphology of the oxide grains: (a) spherical grains; (b) cubical grains; and (c) flaked grains. . . . .	105
7.11	Optical microscopic image of Zr-2.5Nb-H alloy showing hydrides (H-Zr phases)). . . . .	106
7.12	EIS plots: (a) Nyquist plots; and (b) Bode plots. . . . .	107
7.13	Potentiodynamic polarization plots: (a) Variation of OCP with time; and (b) Tafel plots. . . . .	108
7.14	FESEM micrographs of the corroded surface of: (a) U- Zr-2.5Nb alloy; and (b) Zr-2.5Nb-H alloy. . . . .	109
7.15	Schematic representation of the chemical reactions during the corrosion process. . . . .	112

7.16 Schematic representation of the possible corrosion mechanism of Zr-2.5Nb using: (a) electrochemical circuit; and (b) LiOH-Zr-alloy interface during corrosion. . . . . 112

# List of Tables

3.1	Details of experimental parameters for self-mated Zr-4 alloy. . . . .	28
3.2	Details of experimental parameters for Zr-2.5Nb alloy against SS-410. . . . .	29
4.1	Mechanical properties of Zr-4 alloy and SS-410. . . . .	39
6.1	Mechanical properties of Zr-2.5Nb alloy (hydride and unhydrided.) . . . . .	82
7.1	Output values of different electrical elements of the circuit for the corrosion of Zr-4 alloy exposed to the water without LiOH (7 pH). . . . .	94
7.2	Output values of different electrical elements of the circuit for the corrosion of Zr-4 alloy exposed to the water with 0.2 M LiOH (10.4 pH). . . . .	95
7.3	Output values of different electrical elements of the circuit for the corrosion of Zr-4 alloy exposed to the water with 5 M LiOH (11.4 pH). . . . .	95
7.4	Estimated values of corrosion parameters: $E_{corr}$ (V), $i_{corr}$ ( $\text{Acm}^{-2}$ ) and corrosion rate using potentiodynamic polarization experiments for Zr-4 alloy. . . . .	96
7.5	Output values of different electrical elements of the circuit for the corrosion of Zr-2.5Nb alloy exposed to the water without LiOH (7 pH). . . . .	98
7.6	Output values of different electrical elements of the circuit for the corrosion of Zr-2.5Nb alloy exposed to the water with 0.2 M LiOH (10.4 pH). . . . .	99
7.7	Output values of different electrical elements of the circuit for the corrosion of Zr-2.5Nb alloy exposed to the water with 5 M LiOH (11.4 pH). . . . .	100
7.8	Estimated values of corrosion parameters: $E_{corr}$ (V), $i_{corr}$ ( $\text{Acm}^{-2}$ ) and corrosion rate using potentiodynamic polarization experiments for Zr-2.5Nb alloy. . . . .	101
7.9	Output values of different electrical elements of the circuit for the corrosion of Zr-2.5Nb-H alloy exposed to the water with 0.2 M LiOH (10.4 pH). . . . .	107
7.10	Estimated values of corrosion parameters: $E_{corr}$ (V), $i_{corr}$ ( $\text{Acm}^{-2}$ ) and corrosion rate using potentiodynamic polarization experiments for Zr-2.5Nb-H alloy. . . . .	108

# Abbreviations

<b>PHWRs</b>	<b>P</b> ressurized <b>H</b> eavy <b>W</b> ater <b>R</b> eactors
<b>LPIS</b>	<b>L</b> iquid <b>P</b> oison <b>I</b> njection <b>S</b> ystem
<b>Zr-alloys or Zircalloys</b>	<b>Z</b> irconium <b>a</b> alloys
<b>Zr-4 alloy</b>	<b>Z</b> ircaloy-4
<b>Zr-2.5Nb alloy</b>	<b>U</b> nhydrided or as-received <b>Zr-2.5Nb</b> alloy
<b>Zr-2.5Nb-H alloy</b>	<b>H</b> ydrided <b>Zr-2.5Nb</b> alloy
<b>Zr-matrix</b>	<b>Z</b> irconium <b>m</b> atrix
<b>Zr-H phase</b>	<b>Z</b> irconium <b>H</b> ydride <b>p</b> hase
<b>Wt.</b>	<b>W</b> eight
<b>BCC</b>	<b>B</b> ody <b>C</b> entered <b>C</b> ubic
<b>HCP</b>	<b>H</b> exagonal <b>C</b> losed <b>P</b> acked
<b>Avg.</b>	<b>A</b> verage
<b>COF</b>	<b>C</b> oefficient of <b>F</b> riction
<b>w.r.t.</b>	<b>W</b> ith respect to
<b>Sp. wear rate</b>	<b>S</b> pecific wear rate
<b>Tribo-experiments</b>	<b>T</b> ribological experiments
<b>Tribo-corrosion</b>	<b>C</b> orrosion during wear
<b>Fretting-corrosion</b>	<b>C</b> orrosion during fretting wear
<b>RT</b>	<b>R</b> oom <b>T</b> emperature
<b>HT</b>	<b>H</b> igh <b>T</b> emperature
<b>PPM</b>	<b>P</b> arts <b>P</b> er <b>m</b> illion
<b>OFAT</b>	<b>O</b> ne <b>F</b> actor at <b>A</b> <b>T</b> ime
<b>AFM</b>	<b>A</b> tomical <b>F</b> orce <b>M</b> icroscopy
<b>DLC tip</b>	<b>D</b> iamond <b>L</b> ike <b>C</b> arbon tip
<b>SEM</b>	<b>S</b> canning <b>E</b> lectron <b>M</b> icroscopy
<b>FESEM</b>	<b>F</b> ield <b>E</b> mission <b>S</b> canning <b>E</b> lectron <b>M</b> icroscopy
<b>EDS</b>	<b>E</b> nergy <b>D</b> isperssive <b>S</b> pectroscopy

<b>XPS</b>	<b>X-ray Photon Spectroscopy</b>
<b>VMC</b>	<b>Vertical Milling Center</b>
<b>EIS</b>	<b>Electrochemical Impedance Spectroscopy</b>
<b>OCP</b>	<b>Open Circuit Potential</b>
<b>LiOH</b>	<b>Lithium Hydroxide</b>
<b>KOH</b>	<b>Potassium Hydroxide</b>
<b>H<sub>3</sub>BO<sub>3</sub></b>	<b>Boric Acid</b>
<b>pH</b>	<b>Potential of Hydrogen</b>
<b>Conc.</b>	<b>Concentration</b>
<b>R<sub>S</sub></b>	<b>Solution Resistance</b>
<b>R<sub>CT</sub></b>	<b>Charge Transfer Resistance</b>
<b>R<sub>out</sub></b>	<b>Outer oxide layer Resistance</b>
<b>R<sub>in</sub></b>	<b>Inner oxide layer Resistance</b>
<b>C<sub>CT</sub></b>	<b>Charge Transfer Capacitance</b>
<b>C<sub>out</sub></b>	<b>Outer oxide layer Capacitance</b>
<b>C<sub>in</sub></b>	<b>Inner oxide layer Capacitance</b>
<b>CPE<sub>out</sub></b>	<b>Constant Phase Element for outer oxide layer</b>
<b>CPE<sub>in</sub></b>	<b>Constant Phase Element for inner oxide layer</b>

# Symbols

$f$	Frequency
$\omega$	Angular frequency
$^{\circ}\text{C}$	Degree celcius
$\Omega$	Ohm
$\mu$	micro
n	nano
%	Percent
h	Hour
M	Molar and Megha